ASIAN JOURNAL OF PHARMACEUTICAL AND CLINICAL RESEARCH

INNOVARE ACADEMIC SCIENCES
Knowledge to Innovation

Vol 18, Issue 11, 2025

Online - 2455-3891
Print - 0974-2441

Research Article

MECHANISM OF ANTIMICROBIAL ACTION OF SINAPIC ACID INCORPORATED IRON OXIDE NANOFORMULATION AGAINST ORAL PATHOGENS

S. REVATHI[1], J. KALAIMATHI[1]*, M. SURIYA[1], J. DEENA MOL[1], R. KARTHIKA[1], K. SURESH[2], S. RAJESHKUMAR[3]

[1]PG and Research Department of Biochemistry, Theivanai Ammal College for Women (Autonomous), Affiliated to Annamalai University, Villupuram, Tamil Nadu, India, [2]Department of Biotechnology and Biochemistry, Annamalai University, Chidambaram, Tamil Nadu, India, [3]Nanobiomedicine Lab, Centre for Global Health Research, Saveetha Medical Collegeand Hospitals, Saveetha Institute of Medical and Technical Sciences, Chennai, Tamil Nadu, India

***Corresponding Author: Dr. J. Kalaimathi; Email: jkalaimathi1978@gmail.com**

Received: 17 July 2025, Revised and Accepted: 29 September 2025

ABSTRACT

Objective: This study aimed to synthesize and characterize sinapic acid-incorporated Fe_2O_3 nanoparticles (NPs) and to evaluate their antimicrobial mechanism of action against key oral pathogens.

Methods: Fe_2O_3 NPs were synthesized using cinnamon extract and subsequently functionalized with sinapic acid. The nanoformulation was characterized using ultraviolet (UV)–visible spectroscopy, Fourier transform infrared spectroscopy (FTIR), and transmission electron microscopy (TEM) to confirm particle formation, surface functionalization, and morphology. Antimicrobial activity was assessed through agar well diffusion, time-kill curve, protein leakage, and cytoplasmic leakage assays against *Streptococcus mutans*, *Lactobacillus spp.*, *Candida albicans*, *Staphylococcus aureus*, and *Enterococcus faecalis*.

Results: UV–visible spectra showed a characteristic absorption peak near 350 nm, confirming NP formation, while FTIR spectra indicated the presence of phenolic functional groups stabilizing the surface. TEM analysis revealed quasi-spherical NPs with an average size of ~20 nm. The nanoformulation displayed concentration-dependent antimicrobial activity, with *S. mutans* and *Lactobacillus spp.* showing inhibition zones >40 mm at 150 µg/mL. Time-kill assays demonstrated rapid reduction of microbial load, while leakage assays confirmed significant protein and cytoplasmic efflux, indicative of membrane disruption.

Conclusion: Sinapic acid-incorporated Fe_2O_3 NPs exert antimicrobial activity through a dual mechanism involving membrane disruption and reactive oxygen species (ROS) generation. Their nanoscale size, stability, and functionalization enhance efficacy compared to plain Fe_2O_3 NPs. These findings highlight their potential for applications in oral healthcare formulations and localized antimicrobial therapies, though further validation of ROS mechanisms and cytotoxicity is recommended.

Keywords: Sinapic acid, Fe_2O_3 nanoparticles, Antimicrobial activity, Oral pathogens.

 DOI: http://dx.doi.org/10.22159/ajpcr.2025v18i11.55991 Journal homepage: https://innovareacademics.in/journals/index.php/ajpcr

INTRODUCTION

Antimicrobial resistance has become a critical global health issue, complicating the effective treatment of bacterial and fungal infections [1]. The rise in resistance to conventional antibiotics has led to increased morbidity, mortality, and economic burden, necessitating the exploration of innovative therapeutic strategies [2]. Oral pathogens, in particular, pose a significant challenge due to their ability to form resilient biofilms and develop resistance, contributing to infections such as dental caries, periodontal disease, and systemic complications. Addressing these challenges requires a multidisciplinary approach, including the development of novel antimicrobial agents with enhanced efficacy and safety [3].

The oral cavity harbors a complex microbial community, with certain pathogens playing key roles in the onset and progression of oral diseases. *Streptococcus mutans* is a primary contributor to dental caries due to its acidogenic and aciduric properties. Similarly, *Lactobacillus spp. species* exacerbate the cariogenic process by thriving in acidic environments [4]. Fungal pathogens like *Candida albicans* complicate periodontal disease through biofilm formation and resistance to conventional treatments. Other pathogens such as *Staphylococcus aureus* and *Enterococcus faecalis* are associated with systemic infections, root canal failures, and persistent endodontic infections, highlighting the need for effective antimicrobial interventions [5,6].

Iron oxide nanoparticles (Fe_2O_3 NPs) have garnered attention for their unique physicochemical properties, including a high surface area-to-volume ratio, magnetic characteristics, and biocompatibility [7]. These properties make Fe_2O_3 NPs suitable for biomedical applications such as drug delivery and antimicrobial therapies [8]. Their mechanisms of action include disrupting microbial membranes and generating reactive oxygen species (ROS), which damage essential cellular components like DNA, proteins, and lipids. These multifaceted mechanisms provide a robust approach to combat resistant pathogens [9,10].

Sinapic acid, a natural phenolic compound, possesses antioxidant, antimicrobial, and anti- inflammatory properties [11,37]. When incorporated into Fe_2O_3 NPs, sinapic acid enhances NP stability, prevents aggregation, and facilitates increased ROS generation [12]. The synergy between sinapic acid and Fe_2O_3NPs amplifies their antimicrobial efficacy while maintaining biocompatibility, making the nanoformulation a promising candidate for combating infections caused by resilient oral pathogens [8,13].

This study aims to investigate the antimicrobial mechanism of action of sinapic acid- incorporated Fe_2O_3 NPs against clinically significant

oral pathogens. By employing assays such as agar well diffusion, time-kill curve, protein leakage, and cytoplasmic leakage analysis, the study seeks to elucidate the interaction between these NPs and microbial cells, providing insights into their potential applications in oral healthcare and beyond.

MATERIALS AND METHODS

In this study, the Fe_2O_3 NPs were synthesized using cinnamon extract as a natural reducing and stabilizing agent in the green synthesis process. Following this step, the NPs were subsequently functionalized with sinapic acid to enhance stability and antimicrobial efficacy. Thus, cinnamon extract served as the initial biogenic reducing medium, while sinapic acid was incorporated afterward as a capping and functionalizing agent.

Preparation of cinnamon extract

To prepare the cinnamon extract for synthesizing Fe_2O_3 NPs, 1 g of dried cinnamon was added to 100 mL of distilled water. The mixture was heated on a mantle at 60–70°C for 15–20 min to facilitate the extraction of bioactive compounds. The solution was then filtered using Whatman No. 1 filter paper to remove any particulate matter. The filtered extract was stored at 4°C to preserve its active components for NP synthesis.

Synthesis of Fe_2O_3 NPs

For the synthesis of Fe_2O_3 NPs, 30 mM of iron chloride was dissolved in 50 mL of distilled water to prepare the precursor solution. An equal volume (50 mL) of cinnamon extract was added to the solution, providing reducing and stabilizing agents. The reaction mixture was stirred continuously at 600 rpm on a magnetic stirrer for24–48 h stop romote NP formation. The progress of the synthesis was monitored using a ultraviolet (UV)-visible double-beam spectrophotometer to detect characteristic absorbance peaks indicative of Fe_2O_3NPs formation. Upon completion, the NP solution was centrifuged at 8000 rpm for 10 min to separate the Fe_2O_3NPs (pellet) from the supernatant. The pellet was collected, washed, and stored in an airtight Eppendorf tube for further use.

Functionalization of Fe_2O_3NPs with sinapic acid

To prepare the sinapic acid-Fe_2O_3NPs, 100 mg of sinapic acid was dissolved in 1 mL of DMSO and 4 mL of PBS to create a 5 mL solution. This solution was mixed using an orbital shaker for 1 h to ensure uniform dispersion. Subsequently, 1 mL of the sinapic acid solution was added to 1 mL of Fe_2O_3 NPs and sonicated for 30 min to achieve a stable dispersion of sinapic acid onto the NPs. The final nanoformulation was stored for subsequent analysis and antimicrobial testing.

Characterization

The synthesized Fe_2O_3 NPs incorporated with sinapic acid were subjected to physicochemical characterization. UV–visible spectroscopy was performed using a double-beam UV–visible spectrophotometer (Shimadzu UV-1800, Japan) in the range of 200–800 nm to monitor NP formation. Fourier transform infrared spectroscopy (FTIR) was carried out using an FTIR spectrometer (Bruker Alpha II, Germany) in the wavenumber range 4000–400 cm^{-1} to identify functional groups involved in NP stabilization. Transmission electron microscopy (TEM) analysis was performed using a JEOL JEM-2100 microscope (Japan) operating at 200 kV to determine morphology and particle size distribution. The samples were prepared by drop-casting the NP suspension on carbon-coated copper grids, followed by drying under vacuum prior to imaging.

Antimicrobial activity evaluation

Agar well diffusion assay

The antimicrobial activity of sinapic acid-incorporated Fe_2O_3 NPs was evaluated using the agar well diffusion assay. Standardized inoculums of oral pathogens, including *S. mutans*, *Lactobacillus spp.*, *C. albicans*, *S. aureus*, and *E. faecalis*, were prepared to match the 0.5 McFarland turbidity standard (~10^6 CFU/mL). The inoculums were spread evenly on solidified Mueller-Hinton agar plates, and 9mm wells were punched into the agar using a sterile tip. The wells were filled with 100 µL of Fe_2O_3 NP suspensions at concentrations of 25, 50, and 100 µg/mL. Standard antimicrobial agents (amoxyrite for bacteria and fluconazole for fungi) and controls were included for comparison. Plates were incubated at 37°C for 24 h (bacteria) or 28°C for 48 h (fungi), and the zones of inhibition were measured.

Time-kill curve assay

The time-kill curve assay assessed the bactericidal and fungicidal activity of the NPs. Microbial cultures were standardized to~10^6CFU/mL and treated with sinapic acid incorporated Fe_2O_3 NPs at 25, 50, and 100 µg/mL. Standard agents (amoxyrite for bacteria and fluconazole for fungi) and untreated controls were included for comparison. The samples were incubated at 37°C with gentle shaking. At 0, 1, 2, 3, 4, and 5 h, 100 µL aliquots were withdrawn, and their optical density (OD) at 600 nm was measured using an ELISA reader to quantify microbial growth reduction over time.

Protein and cytoplasmic leakage analysis

To explore the mechanism of action, protein and cytoplasmic leakage assays were conducted. Microbial cultures were exposed to sinapic acid incorporated Fe_2O_3 NPs at 25, 50, and 100 µg/mL. The supernatant of treated cultures was collected, and protein leakage was quantified by measuring OD at 280 nm. Cytoplasmic leakage was determined by measuring OD at 260 nm, indicating nucleic acid release. Results were compared to the control (untreated pathogens) and standard agents (amoxyrite for bacteria and fluconazole for fungi) to confirm membrane disruption and cellular damage.

Statistical analysis

All experiments were performed in triplicate (n=3), and results are expressed as mean±standard deviation (SD). Statistical analysis was carried out using GraphPad Prism version 8.0.1 (GraphPad Software, USA). One-way analysis of variance (ANOVA) followed by Tukey's *post hoc* test was employed to compare differences between groups. A $p<0.05$ was considered statistically significant.

RESULT

UV-visible spectroscopy

The results, as illustrated in Fig. 1, demonstrated a characteristic absorption peak near 350 nm, indicative of iron oxide NP formation. The absorbance values increased with time, showing a peak intensity at 24 h, suggesting enhanced particle formation and stability. Specifically, at 3 h, the absorbance was relatively low, indicating the initial stages of NP nucleation. By 12 h, there was a noticeable increase in absorbance, showing a significant progression in NP growth. At 24 h, the absorbance reached its highest point, suggesting that the NPs had achieved optimal formation and stability. The spectral profile and peak shift suggest successful synthesis of Fe_2O_3 NPs with sinapic acid stabilization, and the time-dependent increase in absorbance aligns with the anticipated

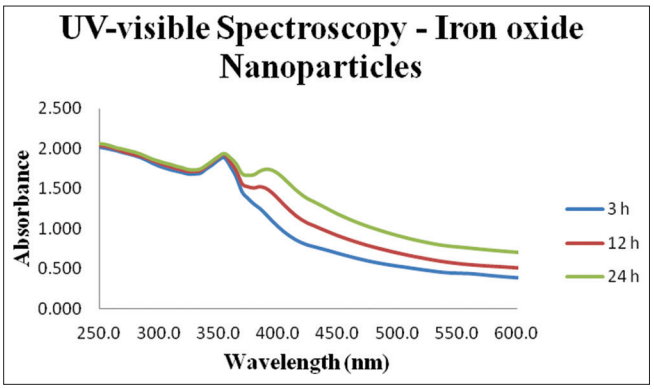

Fig. 1: Fe_2O_3 nanoparticles -sinapic acid nano formulation- ultraviolet -visible spectrum

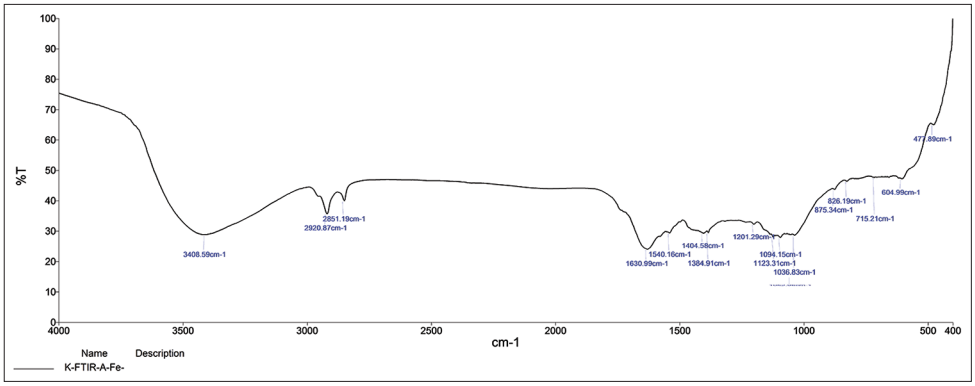

Fig. 2: Fe_2O_3 nanoparticles formulated with sinapic acid-fourier transform infrared spectroscopy spectrum

NP maturation process. This observation supports the effectiveness of sinapic acid and cinnamon extract in facilitating the green synthesis and stabilization of iron oxide NPs.

FT-IR

The spectrum displayed a broad peak around 3400 cm^{-1}, corresponding to O–H stretching vibrations, indicating hydroxyl groups likely from sinapic acid or surface-bound water, contributing to NP stabilization. A distinct absorption band near 1630 cm^{-1} was attributed to C=O stretching, suggesting the involvement of sinapic acid's carbonyl groups in binding to the Fe_2O_3 surface. Additional peaks at approximately 1380 cm^{-1} and 1050 cm^{-1} were assigned to C–H bending and C–O stretching vibrations, respectively, confirming the presence of organic moieties from sinapic acid on the NP surface. The region below 1000 cm^{-1} revealed characteristic Fe–O stretching vibrations, confirming the successful formation of iron oxide NPs. Overall, the FTIR results validate the effective synthesis and functionalization of Fe_2O_3 NPs with sinapic acid, highlighting its dual role in NP formation and stabilization, essential for biomedical applications.

TEM

TEM images (Fig. 3a and b) showed that the NPs possess a quasi-spherical shape with slight agglomeration-typical for green-synthesized nanomaterials. At 210,000× magnification, the particles appeared dense and uniformly shaped, with an average diameter of ~20 nm. Higher magnification (300,000×) confirmed a consistent size and well-defined edges, indicating uniform distribution and controlled synthesis. The nanoscale size and stable morphology suggest that sinapic acid plays a key role in preventing excessive growth and aggregation during NP formation. Overall, the TEM results confirm the successful synthesis of ~20 nm Fe_2O_3 NPs with a stable, quasi-spherical structure-properties that are favorable for biomedical applications due to improved surface area, cellular uptake, and biocompatibility.

Antimicrobial activity

The antimicrobial activity of the NPs was confirmed by agar well diffusion (Fig. 4). Distinct zones of inhibition were observed in a concentration-dependent manner. Specifically, *S. mutans* (Fig. 4a) exhibited a maximum inhibition zone of 42 mm at 150 µg/mL, while *C. albicans* (Fig. 4b) showed a zone of 37 mm. *E. faecalis* (Fig. 4c) displayed moderate inhibition (28 mm at 150 µg/mL), whereas *S. aureus* (Fig. 4d) showed zones of 30–35 mm depending on concentration. *Lactobacillus spp.* (Fig. 4e) exhibited significant inhibition, with a maximum zone of 40 mm at 150 µg/mL. The corresponding quantitative analysis of inhibition zones is shown in Fig. 5. The differences in inhibition zones across concentrations (50, 100, 150 µg/mL) were statistically significant for all pathogens ($p<0.05$, ANOVA with Tukey's test), confirming concentration-dependent activity.

Time kill curve assay

The time-kill curve assay was conducted to evaluate the antimicrobial efficacy of sinapic acid-incorporated Fe_2O_3 NPs at concentrations

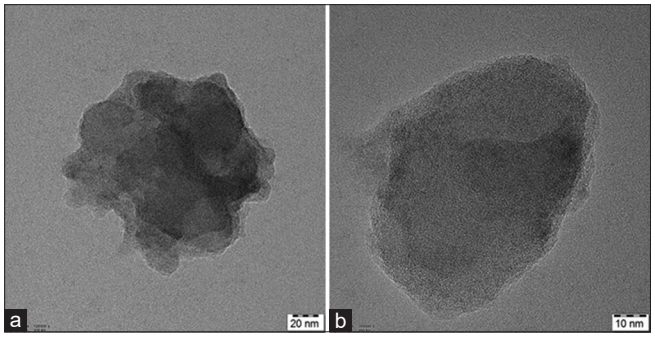

Fig. 3: Fe_2O_3 nanoparticles -sinapic acid nanoformulation transmission electron microscopy images showing (a) aggregated nanostructures at 20 nm scale and (b) individual nanoparticle morphology at 10 nm scale

of 25, 50, and 100 µg/mL against various oral pathogens, including *Lactobacillus spp.*, *C. albicans*, *S. aureus*, *E. faecalis*, and *S. mutans*. The standard control used in the assay was cinnamon extract, while untreated samples served as the negative control. The results, depicted in Fig. 6, highlight the concentration-dependent antimicrobial activity over a 4-h period.

For *Lactobacillus spp.*, the initial CFU count decreased slightly across all concentrations, with the 100 µg/mL concentration showing the most pronounced reduction in bacterial count, closely aligning with the standard control by the end of the 4-h period. The 25 and 50 µg/mL concentrations demonstrated moderate reduction but showed slight regrowth after the 2-h mark, though still below the control level.

In the case of *C. albicans*, the 100 µg/mL concentration exhibited strong antimicrobial activity, significantly reducing CFU counts over the 4-h period, achieving similar results to the standard control. The 50 µg/mL concentration also effectively lowered the CFU count but less markedly than the highest concentration. The 25 µg/mL concentration showed the least reduction among the tested concentrations, indicating a limited effect compared to the standard control.

For *S. aureus*, all concentrations (25, 50, and 100 µg/mL) demonstrated a steady decline in CFU count over time, with the 100 µg/mL concentration resulting in the most substantial bacterial reduction, comparable to the standard. The 50 µg/mL concentration exhibited moderate antimicrobial activity, while the 25 µg/mL concentration showed a minimal reduction in CFU counts, with slight regrowth noted after 3 h. In the case of *E. faecalis*, the higher concentrations (50 and 100 µg/mL) maintained a consistent reduction in CFU counts, closely matching the standard control's performance. The 100 µg/mL concentration proved to be most effective, while the 25 µg/mL concentration displayed limited activity, showing minimal reduction in CFU counts over the 4-h period.

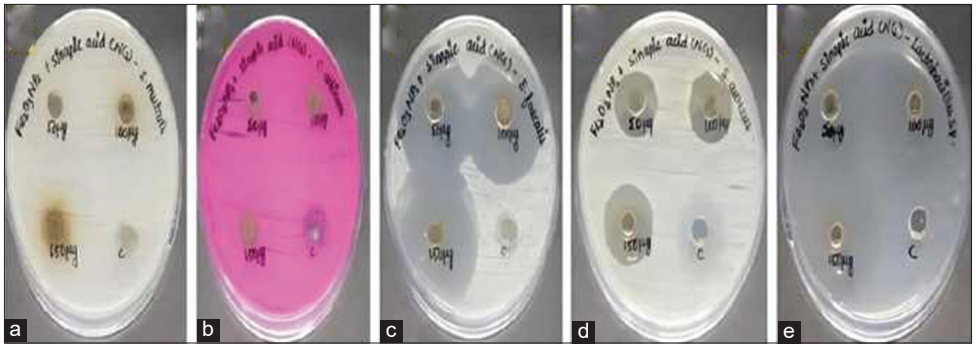

Fig. 4: Agar well diffusion assay demonstrating the antimicrobial activity of sinapic acid-incorporated Fe_2O_3 nanoparticles against oral pathogens at different concentrations (50 µg/mL, 100 µg/mL, and 150 µg/mL) and a control (C). (a) *Streptococcus mutans*, (b) *Candida albicans*, (c) *Enterococcus faecalis*, (d) *Staphylococcus aureus*, and (e) *Lactobacillus spp*

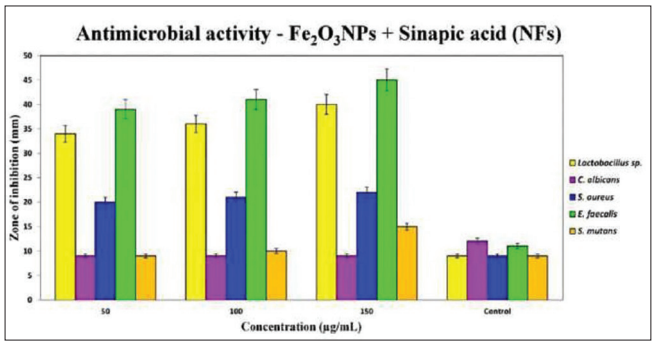

Fig. 5: Antimicrobial activity of sinapic acid-incorporated Fe_2O_3 nanoparticles against oral pathogens (*Lactobacillus spp.*, *Candida. albicans*, *Staphylococcus aureus*, *Enterococcus faecalis*, and *Streptococcus mutans*) measured by agar well diffusion assay. Data are presented as mean±standard deviation (n=3). Statistical significance was determined by one-way analysis of variance with Tukey's *post hoc* test (p<0.05)

Finally, for *S. mutans*, a notable decline in CFU count was observed at the 100 µg/mL concentration, which demonstrated effectiveness comparable to the standard control. The 50 µg/mL concentration provided moderate bacterial suppression, whereas the 25 µg/mL concentration showed minimal antimicrobial impact with slight bacterial regrowth over time.

Significant differences ($p<0.05$) were observed between treated and control groups at each time point, with higher concentrations (100 and 150 µg/mL) showing faster microbial killing kinetics.

Lower concentrations (25 and 50 µg/mL) demonstrated varying levels of activity, generally achieving moderate reduction without complete suppression, especially in longer incubation periods.

Mechanism of antimicrobial activity protein leakage analysis

The protein leakage analysis was conducted to evaluate the membrane-disruptive action of Fe_2O_3 NPs incorporated with sinapic acid against various oral pathogens. This assay measured the OD of leaked proteins in the supernatant at different concentrations of the nanoformulation (25, 50, and 100 µg/mL), along with standard and control groups.

The results showed a concentration-dependent increase in protein leakage across all tested pathogens, indicating membrane damage induced by Fe_2O_3 NPs. At the lowest concentration (25µg/mL), the optical density values for protein leakage were modest, ranging between 0.45 and 0.55 across pathogens. However, at 50 µg/mL, the leakage levels increased, with OD values approaching those of the standard. This trend continued at the highest concentration (100 µg/mL), where the protein leakage reached its peak, showing values similar to or slightly exceeding the standard, particularly for *E. faecalis* and *S. mutans*, which had the highest protein leakage, with optical densities close to 0.6.

Protein leakage increased significantly in a concentration-dependent manner ($p<0.05$) compared to untreated controls for all tested pathogens. These findings suggest that Fe_2O_3 NPs induce antimicrobial activity by disrupting the cellular membrane integrity, leading to leakage of intracellular proteins. This mechanism highlights the potential of Fe_2O_3 NPs as a potent antimicrobial agent that compromises bacterial and fungal cell membranes, thereby inhibiting pathogen survival.

Cytoplasmic leakage analysis

The cytoplasmic leakage analysis was conducted to assess the extent of cellular damage caused by Fe_2O_3 NPs incorporated with sinapic acid against selected oral pathogens. The assay measured the OD of cytoplasmic contents released into the surrounding medium at different concentrations of the nanoformulation (25, 50, and 100 µg/mL), along with standard and control groups.

OD260 measurements revealed significant cytoplasmic leakage at 50 and 100 µg/mL compared with controls ($p<0.05$), supporting membrane disruption as a primary mechanism. At 25 µg/mL, moderate cytoplasmic leakage was observed, with OD values ranging from 0.45 to 0.55. When the concentration was increased to 50 µg/mL, the leakage levels rose, with optical densities approaching those seen in the standard control, particularly for *Lactobacillus spp.* and *E. faecalis*, which exhibited the highest OD readings among the pathogens.

The highest concentration, 100 µg/mL, demonstrated the most pronounced cytoplasmic leakage, with OD values comparable to or slightly exceeding the standard control. This trend was most evident in *S. aureus* and *S. mutans*, where OD readings approached 0.65–0.7, indicating significant membrane disruption. The control group, which lacked Fe_2O_3 NPs, displayed minimal cytoplasmic leakage, confirming the essential role of the Fe_2O_3 NPs in inducing cellular damage.

These findings indicate that Fe_2O_3 NPs cause membrane disruption leading to cytoplasmic leakage, contributing to their antimicrobial action against oral pathogens. The results highlight the ability of Fe_2O_3 NPs to compromise the structural integrity of microbial cells, thereby inhibiting their growth and survival.

DISCUSSION

The physicochemical characterization of sinapic acid–incorporated Fe_2O_3 NPs confirmed their successful synthesis and stability. UV–visible spectroscopy showed a distinct absorption peak consistent with NP formation, while FTIR spectra verified the presence of phenolic functional groups from sinapic acid on the NP surface, confirming functionalization and stabilization (Fig. 2). TEM analysis further revealed quasi-spherical NPs with an average size of ~20 nm, a morphology favorable for cellular uptake and biofilm penetration.

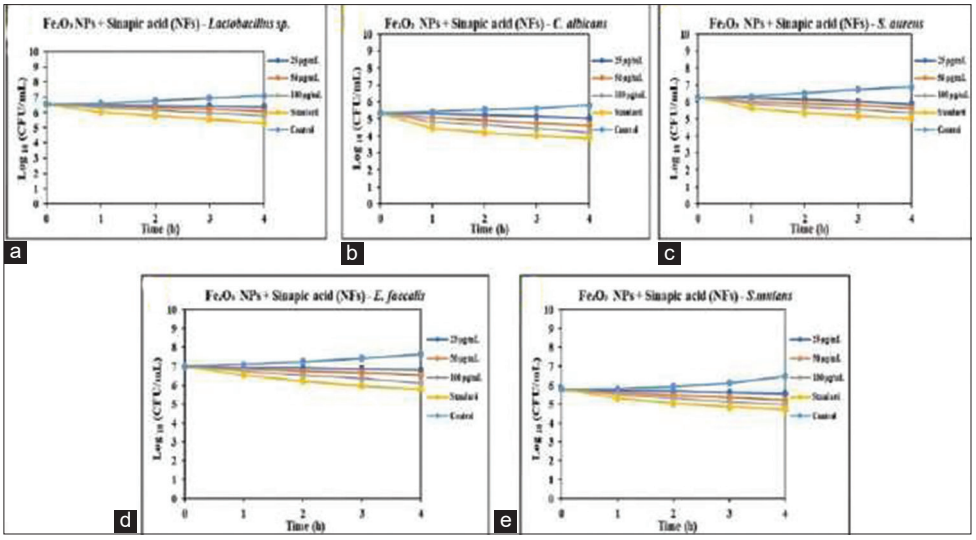

Fig. 6: Time-kill curve assay showing the antimicrobial activity of sinapic acid-incorporated Fe_2O_3 nanoparticles against oral pathogens: (a) *Lactobacillus spp.*, (b) *Candida albicans*, (c) *Staphylococcus aureus*, (d) *Enterococcus faecalis*, and (e) *Streptococcus mutans*. Data are presented as mean±standard deviation (n=3). Statistical significance was determined by one-way analysis of variance with Tukey's *post hoc* test ($p<0.05$)

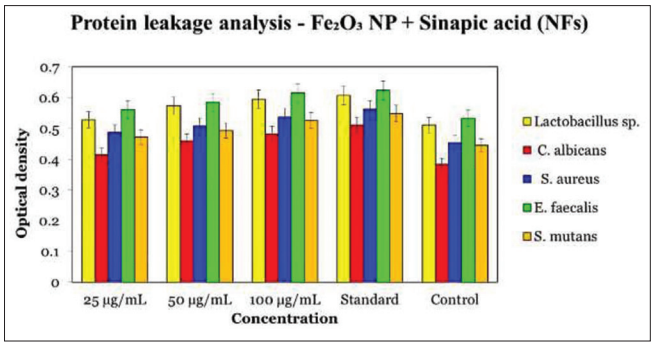

Fig. 7: Protein leakage analysis demonstrating the membrane-disruptive effect of sinapic acid-incorporated Fe_2O_3 nanoparticles against oral pathogens (*Lactobacillus spp.*, *Candida albicans*, *Staphylococcus aureus*, *Enterococcus faecalis*, and *Streptococcus mutans*). Data are presented as mean±standard deviation (n=3). Statistical significance was determined by one-way analysis of variance with Tukey's *post hoc* test ($p<0.05$)

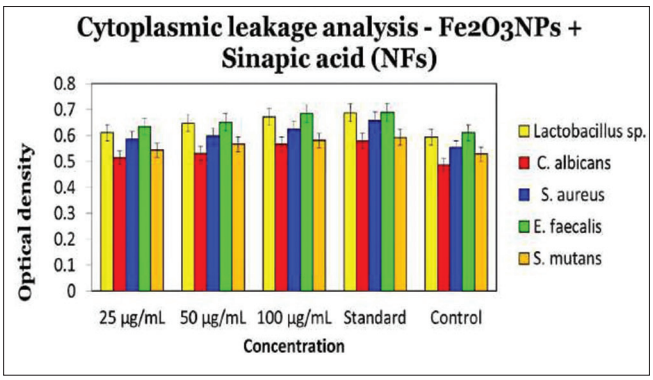

Fig. 8: Cytoplasmic leakage analysis illustrating the membrane-disruptive effects of sinapic acid-incorporated Fe_2O_3 nanoparticles on oral pathogens (*Lactobacillus spp.*, *Candida albicans*, *Staphylococcus aureus*, *Enterococcus faecalis*, and *Streptococcus mutans*). Data are presented as mean±standard deviation (n=3). Statistical significance was determined by one-way analysis of variance with Tukey's *post hoc* test ($p<0.05$)

The nanoscale dimensions also maximize surface area, which is critical for enhancing interactions with microbial membranes and thereby augmenting antimicrobial efficacy [14-16].

The antimicrobial activity of the nanoformulation was comprehensively investigated using agar well diffusion, time-kill kinetics, protein leakage, and cytoplasmic leakage assays. Each assay provided complementary insights into efficacy and mechanism. The agar well diffusion assay demonstrated concentration-dependent inhibition, with *S. mutans* and *Lactobacillus spp.* exhibiting the largest zones exceeding 40 mm at 150 µg/mL, while *C. albicans* and *E. faecalis* displayed smaller inhibition zones, indicating relative resistance. These findings were further supported by quantitative measurements (Fig. 5), where significant differences across concentrations were confirmed by statistical analysis (ANOVA with Tukey's *post hoc* test, $p<0.05$) [15-18].

The time-kill curve assay provided dynamic evidence of antimicrobial kinetics. At 150 µg/mL, a rapid and sustained decline in colony-forming units was observed within 4 h across all pathogens, confirming robust bactericidal and fungicidal activity [19,20]. At lower concentrations (50–100 µg/mL), partial regrowth occurred, suggesting incomplete membrane disruption at suboptimal doses. Importantly, pathogens that showed the highest leakage in subsequent assays-*S. mutans* and *Lactobacillus spp.*,—were also those most rapidly killed, directly linking membrane destabilization with antimicrobial outcomes [21-24].

Protein leakage analysis quantified the extent of membrane disruption caused by the NPs. At 25 µg/mL, modest protein leakage (OD ~0.45) was observed, but levels rose significantly at 50–100 µg/mL, with *S. mutans* and *E. faecalis* showing OD values near 0.6 (Fig. 7). These results align with the inhibition zones and time-kill data, confirming that NP-induced membrane damage correlates with antimicrobial efficacy [25-27]. Cytoplasmic leakage assays further validated this mechanism, showing concentration-dependent nucleic acid release, with peak OD values of 0.65–0.7 for *S. aureus* and *S. mutans* at 100 µg/mL (Fig. 8). The minimal leakage in the control (cinnamon extract) underscores the enhanced effect of sinapic acid functionalization [28,29]. The consistency between protein and cytoplasmic leakage results strengthens the conclusion that membrane disruption is the principal antimicrobial pathway [30].

Taken together, the mechanism of action of sinapic acid–incorporated

Fe_2O_3 NPs appears to be multifaceted. The NPs directly interact with microbial membranes, destabilizing their structural integrity and increasing permeability, which results in the efflux of essential intracellular proteins and nucleic acids. While ROS generation is a well-documented effect of iron oxide NPs, our study did not directly quantify ROS using probes such as DCFH-DA. Thus, ROS should be regarded as a hypothetical secondary mechanism rather than a confirmed pathway. Future studies are required to confirm this possibility [31,32].

The novelty of the present nanoformulation lies in the synergistic contribution of the Fe_2O_3 core and the sinapic acid coating. Compared with plain Fe_2O_3 NPs, sinapic acid enhances stability, prevents aggregation, and likely contributes antimicrobial activity through its phenolic properties, including ROS modulation, metal ion chelation, and metabolic disruption. Other phenolic acid coatings have previously been shown to improve antimicrobial efficacy, but sinapic acid remains underexplored, making this work an incremental advancement in NP-based antimicrobial design [17,32,33].

Despite the promising results, several limitations must be acknowledged. The agar well diffusion assay may underestimate activity due to limited NP diffusion through agar and potential aggregation. The OD-based approach in the time-kill assay may be less reliable for fungal species such as *C. albicans*, which tend to clump. Furthermore, *in vivo* cytotoxicity and oral microbiome effects remain untested. Comprehensive cytotoxicity studies, ROS quantification, and *in vivo* validation will be essential before clinical application [28,33].

Clinical and translational relevance

The broad-spectrum antimicrobial efficacy of sinapic acid–incorporated Fe_2O_3 NPs highlights their potential for oral healthcare applications. Their effectiveness against *S. mutans* and *E. faecalis*-key pathogens in dental caries and endodontic infections suggests their incorporation into oral hygiene formulations such as mouthwashes, toothpastes, gels, and varnishes. Their antifungal activity against *C. albicans* further indicates potential for treating oral candidiasis in immunocompromised individuals. Beyond dentistry, these NPs could also be employed in wound dressings and other localized therapies against antibiotic-resistant infections [34-36].

CONCLUSION

This study establishes sinapic acid-incorporated Fe_2O_3 NPs as an effective antimicrobial agent against a range of oral pathogens, including *S. mutans*, *Lactobacillus spp.*, *C. albicans*, *S. aureus*, and *E. faecalis*. The antimicrobial efficacy, demonstrated through agar well diffusion, time-kill curve, protein leakage, and cytoplasmic leakage analyses, reveals a robust, concentration-dependent activity. At higher concentrations, these NPs caused significant membrane disruption, evidenced by the leakage of intracellular proteins and cytoplasmic contents, leading to microbial cell death. The generation of ROS further enhanced the NPs' bactericidal and fungicidal effects. The incorporation of sinapic acid significantly enhanced the antimicrobial properties of Fe_2O_3 NPs by stabilizing their structure, promoting ROS generation, and synergistically disrupting microbial membranes. *S. mutans* and *Lactobacillus spp.* exhibited the highest sensitivity, highlighting the potential of these NPs in oral healthcare applications.

These findings position sinapic acid-incorporated Fe_2O_3 nanoparticles as promising candidates for use in oral hygiene products, dental restorative materials, and localized antimicrobial therapies, due to their potent antimicrobial properties, biocompatibility, and ability to promote oral health while minimizing side effects associated with conventional treatments. However, further studies are needed to optimize NP formulations, assess biocompatibility, and evaluate long-term impacts on microbial resistance and the oral microbiome. With these advancements, these NPs could provide innovative solutions for addressing microbial infections in oral and medical care.

ACKNOWLEDGMENTS

The authors express their sincere gratitude to the Research Supervisor, Department of Biochemistry, Theivanai Ammal College for Women (Autonomous), Villupuram, for her invaluable guidance, encouragement, and expertise throughout the study. Special appreciation is also extended to the research teams at Saveetha Medical College, Chennai, and Annamalai University, Chidambaram, for their valuable collaborative support.

CONFLICTS OF INTEREST

The authors declare no conflicts of interest.

ETHICAL ISSUES

None.

FUNDING

Nil.

REFERENCES

1. Zhu Y, Wang Y, Zhang S, Li J, Li X, Ying Y, *et al*. Association of polymicrobial interactions with dental caries development and prevention. Front Microbiol. 2023;14:1162380. doi: 10.3389/fmicb.2023.1162380, PMID: 37275173
2. Durand R, Roufegarinejad A, Chandad F, Rompré PH, Voyer R, Michalowicz BS, *et al*. Dental caries are positively associated with periodontal disease severity. Clin Oral Investig. 2019;23(10):3811-9. doi: 10.1007/s00784-019-02810-6, PMID: 30693397
3. Li Y, Xiang Y, Ren H, Zhang C, Hu Z, Leng W, *et al*. Association between periodontitis and dental caries: A systematic review and meta-analysis. Clin Oral Investig. 2024;28(6):306. doi: 10.1007/s00784-024-05687-2, PMID: 38727727
4. Loesche WJ. Microbiology of dental decay and periodontal disease. In: Baron S, editor. Medical Microbiology. 4th ed. Galveston, TX: University of Texas Medical Branch at Galveston; 1996. Available from: https://www.ncbi.nlm.nih.gov/books/NBK8259
5. Zhang JS, Chu CH, Yu OY. Oral microbiome and dental caries development. Dent J (Basel). 2022;10(10):184. doi: 10.3390/dj10100184, PMID: 36285994
6. Vajjiravelu R, Palani B, Shanmugam R, Jayakodi S. Bioinspired nanoparticles mediated from bioactive plants and their therapeutic application in liver cancer. Biomed Mater Devices. 2025;191:1-6. doi: 10.1007/s44174-025-00062-5
7. Giedraitienė A, Ružauskas M, Šiugždinienė R, Tučkutė S, Grigonis K, Milčius D. Development of antibacterial cotton textiles by deposition of Fe_2O_3 nanoparticles using low-temperature plasma sputtering. Nanomaterials (Basel). 2023;13(24):3106. doi: 10.3390/nano13243106, PMID: 38133003
8. Mohamed AT, Hameed RA, El-Moslamy SH, Fareid M, Othman M, Loutfy SA, *et al*. Facile synthesis of Fe_2O_3, Fe_2O_3@CuO and WO_3 nanoparticles: Characterization, structure determination and evaluation of their biological activity. Sci Rep. 2024;14(1):6081. doi: 10.1038/s41598-024-55319-8, PMID: 38480834
9. Gudkov SV, Burmistrov DE, Serov DA, Rebezov MB, Semenova AA, Lisitsyn AB. Do iron oxide nanoparticles have significant antibacterial properties? Antibiotics (Basel). 2021;10(7):884. doi: 10.3390/antibiotics10070884, PMID: 34356805
10. Preeth DR, Shairam M, Suganya N, Hootan R, Kartik R, Pierre K, *et al.* Green synthesis of copper oxide nanoparticles using sinapic acid:An underpinning step towards antiangiogenic therapy for breast cancer. J Biol Inorg Chem. 2019;24(5):633-45. doi: 1007/s00775-019-10 01676-z, PMID: 31230130
11. Raj Preeth D, Shairam M, Suganya N, Hootan R, Kartik R, Pierre K, *et al*. Green synthesis of copper oxide nanoparticles using sinapic acid: An underpinning step towards antiangiogenic therapy for breast cancer. J Biol Inorg Chem. 2019;24(5):633-45. doi: 10.1007/s00775-019-01676-z, PMID: 31230130
12. Torrisi C, Morgante A, Malfa G, Acquaviva R, Castelli F, Pignatello R, *et al*. Sinapic acid release at the cell level by incorporation into nanoparticles: Experimental evidence using biomembrane models. Micro. 2021;1(1):120-8. doi: 10.3390/micro1010009
13. Balagangadharan K, Trivedi R, Vairamani M, Selvamurugan N. Sinapic

acid-loaded chitosan nanoparticles in polycaprolactone electrospun fibers for bone regeneration *in vitro* and *in vivo*. Carbohydr Polym. 2019;216:1-16. doi: 10.1016/j.carbpol.2019.04.002, PMID: 31047045

14. Al-Zahrani FA, Salem SS, Al-Ghamdi HA, Nhari LM, Lin L, El-Shishtawy RM. Green synthesis and antibacterial activity of Ag/Fe_2O_3 nanocomposite using *Buddleja lindleyana* extract. Bioengineering (Basel). 2022;9(9):452. doi: 10.3390/bioengineering9090452, PMID: 36134998
15. Vihodceva S, Šutka A, Sihtmäe M, Rosenberg M, Otsus M, Kurvet I, *et al*. Antibacterial activity of positively and negatively charged hematite (α-Fe_2O_3) nanoparticles to *Escherichia coli*, *Staphylococcus aureus* and *Vibrio fischeri*. Nanomaterials (Basel). 2021;11(3):652. doi: 10.3390/nano11030652, PMID: 33800165
16. Shanmugam R, Tharani M, Abullais SS, Patil SR, Karobari MI. Black seed assisted synthesis, characterization, free radical scavenging, antimicrobial and anti-inflammatory activity of iron oxide nanoparticles. BMC Complement Med Ther. 2024;24(1):241. doi: 10.1186/s12906-024-04552-9, PMID: 38902620
17. Poyraz FŞ, Akbaş G, Duranoğlu D, Acar S, Mansuroğlu B, Ersöz M. Sinapic-acid-loaded nanoparticles optimized via experimental design methods: Cytotoxic, antiapoptotoic, antiproliferative, and antioxidant activity. ACS Omega. 2024;9(39):40329-45. doi: 10.1021/acsomega.4c00216, PMID: 39371991
18. Russo S, Greco G, Sarpietro MG. Assessment of pharmaco-technological parameters of solid lipid nanoparticles as carriers for sinapic acid. Micro. 2023;3(2):510-20. doi: 10.3390/micro3020034
19. Ge X, Cao Z, Chu L. The antioxidant effect of the metal and metal-oxide nanoparticles. Antioxidants (Basel). 2022;11(4):791. doi: 10.3390/antiox11040791, PMID: 35453476
20. Tharani M, Rajeshkumar S, Al-Ghanim KA, Nicoletti M, Sachivkina N, Govindarajan M. *Terminalia chebula*-assisted silver nanoparticles: Biological potential, synthesis, characterization, and ecotoxicity. Biomedicines. 2023;11(5):1472. doi: 10.3390/biomedicines11051472, PMID: 37239143
21. Menichetti A, Mavridi-Printezi A, Mordini D, Montalti M. Effect of size, shape and surface functionalization on the antibacterial activity of silver nanoparticles. J Funct Biomater. 2023;14(5):244. doi: 10.3390/jfb14050244, PMID: 37233354
22. Pallela PN, Ummey S, Ruddaraju LK, Gadi S, Cherukuri CS, Barla S, *et al*. Antibacterial efficacy of green synthesized α-Fe_2O_3 nanoparticles using *Sida cordifolia* plant extract. Heliyon. 2019;5(11):e02765. doi: 10.1016/j.heliyon.2019.e02765, PMID: 31799458
23. Zúñiga-Miranda J, Guerra J, Mueller A, Mayorga-Ramos A, Carrera-Pacheco SE, Barba-Ostria C, *et al*. Iron oxide nanoparticles: Green synthesis and their antimicrobial activity. Nanomaterials (Basel). 2023;13(22):2919. doi: 10.3390/nano13222919, PMID: 37999273
24. Parthasarathy PR, Varshan EI, Shanmugam R. *In vitro* anti-diabetic activity of pomegranate peel extract-mediated strontium nanoparticles. Cureus. 2023;15(12):e51356. doi: 10.7759/cureus.51356
25. Rajeshkumar S, Jayakodi S, Tharani M, Alharbi NS, Thiruvengadam M. Antimicrobial activity of probiotic bacteria-mediated cadmium oxide nanoparticles against fish pathogens. Microb Pathog. 2024;189:106602. doi: 10.1016/j.micpath.2024.106602, PMID: 38408546
26. Rajeshkumar S, Parameswari RP, Sandhiya D, Al-Ghanim KA, Nicoletti M, Govindarajan M. Green synthesis, characterization and bioactivity of *Mangifera indica* seed-wrapped zinc oxide nanoparticles. Molecules. 2023;28(6):2818. doi: 10.3390/molecules28062818, PMID: 36985789
27. Shanmugam R, Munusamy T, Nisha M A, Rajaselin A, Govindharaj S. Exploring the *in vitro* antidiabetic potential of metal oxide nanoparticles synthesized using lemongrass and mint formulation. Cureus. 2024;16(2):e53489. doi: 10.7759/cureus.53489, PMID: 38440044
28. Niazi F, Ali M, Haroon U, Farhana, Kamal A, Rashid T, *et al*. Effect of green Fe_2O_3 nanoparticles in controlling *Fusarium* fruit rot disease of loquat in Pakistan. Braz J Microbiol. 2023;54(3):1341-50. doi: 10.1007/s42770-023-01050-x, PMID: 37400611
29. Mendes AR, Granadeiro CM, Leite A, Pereira E, Teixeira P, Poças F. Optimizing antimicrobial efficacy: Investigating the impact of zinc oxide nanoparticle shape and size. Nanomaterials (Basel). 2024;14(7):638. doi: 10.3390/nano14070638, PMID: 38607172
30. Precupas A, Popa VT. Impact of sinapic acid on bovine serum albumin thermal stability. Int J Mol Sci. 2024;25(2):936. doi: 10.3390/ijms25020936, PMID: 38256010
31. Arif Muhammed R, Mohammed S, Visht S, Omar Yassen A. A review on development of colon targeted drug delivery system. Int J Appl Pharm. 2024;16(2):12-27. doi: 10.22159/ijap.2024v16i2
32. Franco D, Calabrese G, Guglielmino SP, Conoci S. Metal-based nanoparticles: Antibacterial mechanisms and biomedical application. Microorganisms. 2022;10(9):1778. doi: 10.3390/microorganisms10091778, PMID: 36144380
33. Rajeshkumar S, Tharani M, Jeevitha M, Santhoshkumar J. Anticariogenic activity of fresh *Aloe vera* gel mediated copper oxide nanoparticles. Indian J Public Health Res Dev. 2019;10(11):3664. doi: 10.5958/0976-5506.2019.04158.5
34. Sasidharan I, Menon AN. Comparative chemical composition and antimicrobial activity of fresh and dry ginger oils (*Zingiber officinale* Roscoe). Int J Curr Pharm Res. 2010;2(4):40-3.
35. Rani AP, Archana N, Teja PS, Vikas. PM, Sekaran MS. Antimicrobial activity of medicinal plants. Int J Appl Pharm. 2010;2(3):15-21.
36. Palani B, Vajjiravelu R, Shanmugam R, Jayakodi S. A comprehensive review of traditional medicinal plants and their role in ovarian cancer treatment. S Afr J Bot. 2025;181:426-45. doi: 10.1016/j.sajb.2025.04.019
37. Kalaimathi J, Suresh K. Sinapic acid attenuates 7,12-dimethylbenz[a] anthracene-induced oral carcinogenesis by improving the apoptotic associated gene expression in hamsters. Asian J J Pathol Clin Res. 2015;8(6):134-138. ISSN 0974-2441.